

## Euclidean dynamical triangulations revisited

Muhammad Asaduzzaman<sup>\*</sup>

*Department of Physics and Astronomy, University of Iowa, Iowa City, Iowa 52242, USA*

Simon Catterall<sup>†</sup>

*Department of Physics, Syracuse University, Syracuse, New York 13244, USA*

 (Received 9 November 2022; accepted 19 March 2023; published 14 April 2023)

We conduct numerical simulations of a model of four-dimensional quantum gravity in which the path integral over continuum Euclidean metrics is approximated by a sum over combinatorial triangulations. At fixed volume, the model contains a discrete Einstein-Hilbert term with coupling  $\kappa$  and a local measure term with coupling  $\beta$  that weights triangulations according to the number of simplices sharing each vertex. We map out the phase diagram in this two-dimensional parameter space and compute a variety of observables that yield information on the nature of any continuum limit. Our results are consistent with a line of first-order phase transitions with a latent heat that decreases as  $\kappa \rightarrow \infty$ . We find a Hausdorff dimension along the critical line that approaches  $D_H = 4$  for large  $\kappa$  and a spectral dimension consistent with  $D_s = \frac{3}{2}$  at short distances. These results are broadly in agreement with earlier works on Euclidean dynamical triangulation models which utilize degenerate triangulations and/or different measure terms and indicate that such models exhibit a degree of universality.

DOI: [10.1103/PhysRevD.107.074505](https://doi.org/10.1103/PhysRevD.107.074505)

### I. INTRODUCTION

There are many proposals for quantizing four-dimensional gravity (see the reviews [1–4]). Among those, we explore a nonperturbative and background-independent approach known as Euclidean dynamical triangulation (EDT), in which a discrete sum over simplicial manifolds replaces the continuum path integral. This approach is similar in spirit to the causal dynamical triangulation (CDT) program [2,5] after relaxing the causality constraint in the discrete sum over triangulations. Hence unlike CDT, there is no explicit time direction in a triangulation of EDT formulation where a spacelike hypersurface can be identified. In practice, we restrict to triangulations with equal edge lengths and fixed topology. In addition, we only include so-called combinatorial triangulations in the discrete path integral, which guarantees that the neighborhood of each vertex is homomorphic to a 4-ball. This ensures that any  $p$ -simplex in the triangulation is uniquely specified in terms of its vertices. This differs from the recent work by Laiho *et al.* which utilizes an ensemble of degenerate

triangulations, and a different measure term [6–9]. Our work is also complementary to that of Ambjorn *et al.* [10] who employ the same class of triangulations but a different measure term.

The goal of our work has been to provide a detailed picture of the phase diagram of the model and the location of possible phase transitions by simulating the model over a fine grid in the two-dimensional parameter space for three lattice volumes ranging up to  $N_4 = 32,000$  four-simplices. We find evidence for a single critical line separating a crumpled from a branched polymer phase consistent with all earlier studies of similar models. In addition to certain bulk observables, we have focused our attention on the Hausdorff and spectral dimensions at different phases near the transition line and are able to compute these along and transverse to this critical line more systematically than the previous studies [6,7,10].

### II. THE LATTICE MODEL

The partition function of the model for pure gravity takes the form

$$Z = \sum_T \rho(T) e^{-S} \quad (1)$$

where the discrete action  $S$  is given by

$$S = -\kappa N_0 + \lambda N_4 + \gamma(N_4 - V)^2, \quad (2)$$

<sup>\*</sup>masaduzz@syr.edu

<sup>†</sup>smcatter@syr.edu

*Published by the American Physical Society under the terms of the Creative Commons Attribution 4.0 International license. Further distribution of this work must maintain attribution to the author(s) and the published article's title, journal citation, and DOI. Funded by SCOAP<sup>3</sup>.*

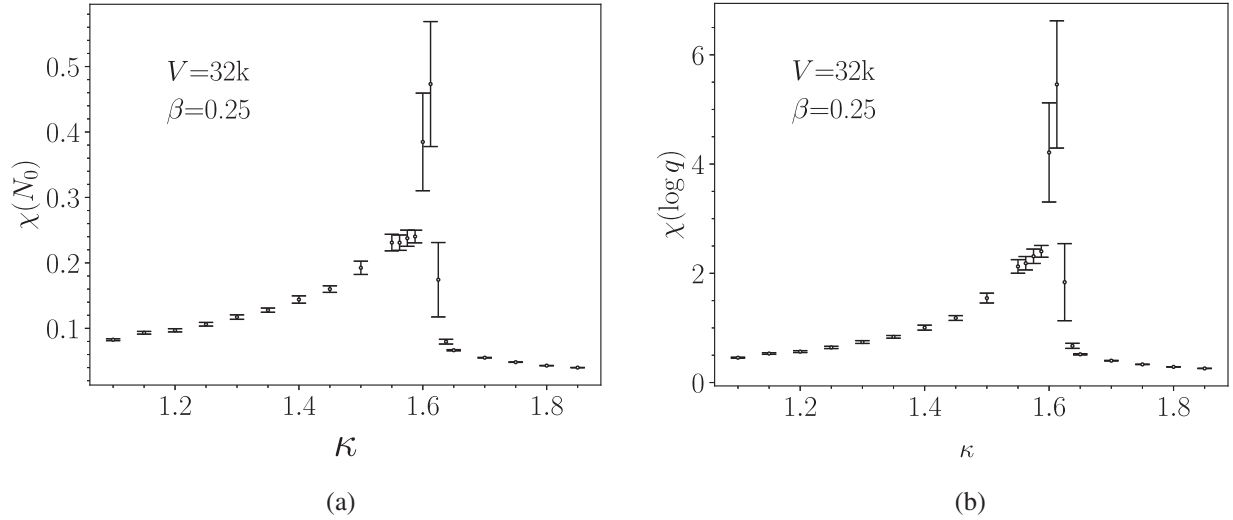


FIG. 1. Susceptibility plots (a)  $\chi_{N_0}$  and (b)  $\chi_{\log q}$  for  $V = 32K$  are shown. The peaked structure near  $\kappa \sim 1.6$  indicates a phase transition.

where the sum runs over all abstract triangulations with fixed (here spherical) topology.<sup>1</sup> The first two terms in the action depend on the number of vertices  $N_0$  and the number of four simplices  $N_4$  arise from using Regge calculus [13,14] to discretize the continuum Einstein-Hilbert action with  $\kappa$  playing the role of the bare Newton constant and  $\lambda$  a bare cosmological constant. The third term plays an auxiliary role in effectively fixing the target volume to  $V$  by tuning  $\lambda$  while still allowing for small fluctuations  $\delta V \sim \frac{1}{\sqrt{V}}$  essential to ensure ergodicity in the Monte Carlo sampling of the triangulations.

The central assumption in this approach to quantum gravity is that the sum over triangulations reproduces, in some appropriate continuum limit, the ill-defined continuum path integral over metrics modulo diffeomorphisms. In two dimensions, this prescription reproduces known results for 2D gravity from Liouville theory and matrix models [15,16] but in higher dimensions reproducing continuum gravity is merely a plausible ansatz.

Most recent works assume that an additional measure term  $\rho(T)$ , which depends on local properties of the triangulation, is needed to ensure this correspondence with continuum gravity remains true [7,10]. Here we employ a new form

$$\rho(T) = \prod_{i=1}^{N_0} q_i^\beta, \quad (3)$$

where  $q_i$  denotes the number of simplices sharing vertex  $i$  and  $\beta$  is a new parameter. The measure term is similar to the

<sup>1</sup>Numerical evidence has been presented in previous studies that the number of possible 4D triangulations of fixed spherical topology is exponentially bounded [11,12] and hence can be controlled by a bare cosmological constant term.

local measure term used in previous studies where the coordination number of the triangles is used [7,10]. It is conjectured that tuning the coupling to such an operator is necessary to restore the continuum symmetries and approach a fixed point where a continuum limit can be taken [10], which describes quantum gravity.

Our work is focused on examining the phase structure of the model in the  $(\kappa, \beta)$  with the goal of searching for critical behavior and locating a region where such a continuum limit exists.

### III. PHASE STRUCTURE

We employ a Monte Carlo algorithm to sample the sum over random triangulations of the four dimensional sphere [17]. Five elementary local moves (“Pachner moves”) which, applied randomly, are known to be sufficient to reach any part of the triangulation space.

Two of the simplest observables that can be used to locate the transition are the node and measure susceptibilities which are defined by

$$\chi_{N_0} = \frac{1}{V} (\langle N_0^2 \rangle - \langle N_0 \rangle^2) \quad (4)$$

$$\chi_{\log q} = \frac{1}{V} (\langle Q^2 \rangle - \langle Q \rangle^2) \quad (5)$$

with  $Q = \frac{1}{N_0} \sum_{i=1}^{N_0} \log q_i$ .

In Fig. 1 we show these as a function of  $\kappa$  at  $\beta = 0.25$  for a lattice of (average) volume  $N_4 = 32,000$ . We used  $10^7$  thermalized triangulations to compute the thermodynamic quantities where we defined a Monte Carlo sweep as an attempt to change the triangulation (using the Pachner moves) 32,000 times by randomly choosing the moves and the associated simplices/subsimplices. Measured quantities

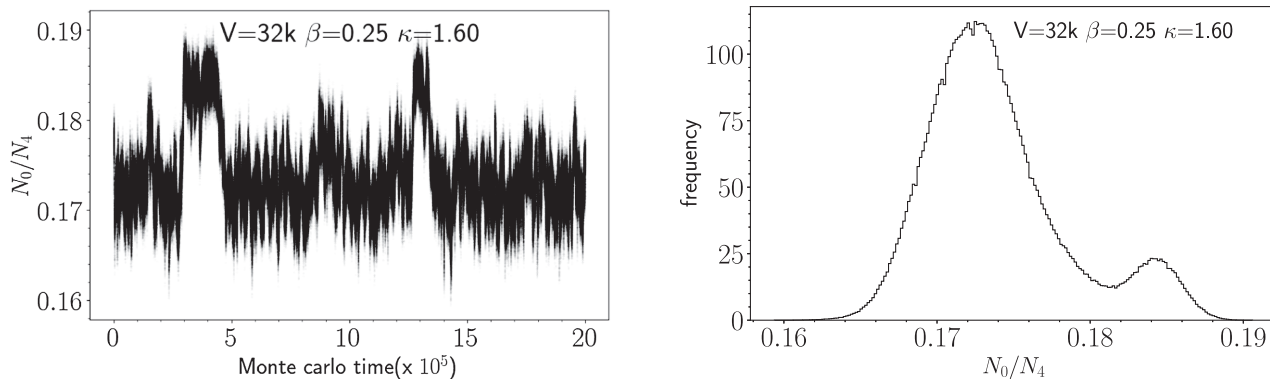


FIG. 2. First-order nature of the transition at  $\beta = 0.25$  can be seen from the (a) Monte Carlo time series for  $N_0/N_4$  and (b) double peak structure of the probability density of  $N_0/N_4$ .

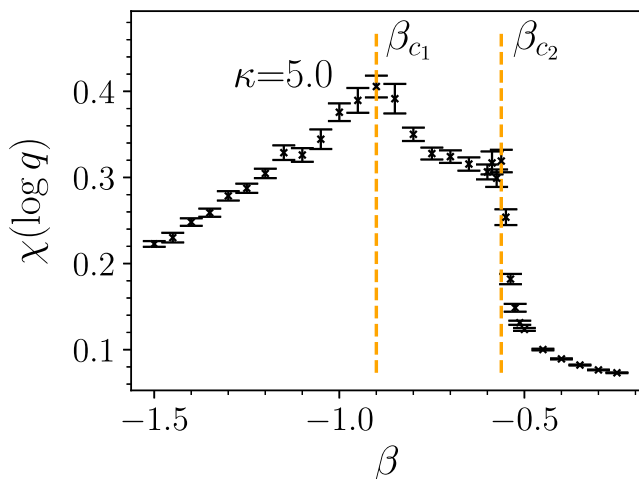


FIG. 3. At large  $\kappa$  two distinctive peaks are observed in the susceptibility plots. Position of the critical points are shown with the vertical lines.

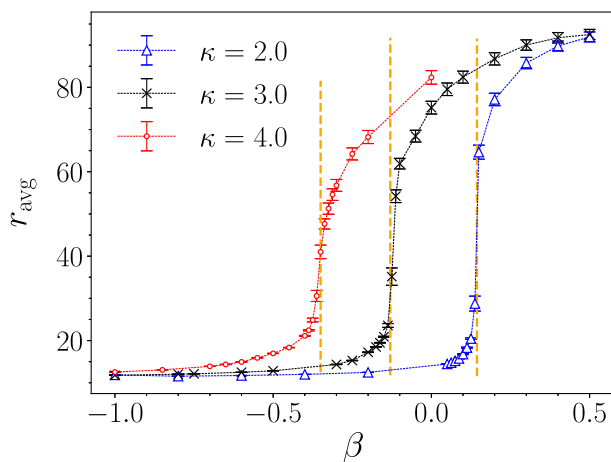


FIG. 4.  $\beta$  dependence of the average radius  $r_{\text{avg}}$  at different fixed values of  $\kappa$ , at a target volume  $V = 32$  K. Vertical lines denote the position of the critical points  $\hat{\beta}_c$  at different gravitational constants  $\kappa$ .

were further blocked afterwards to compute the jackknife errors. The peaks in both susceptibility quantities indicate the presence of a phase transition.

In Fig. 2 we show the Monte Carlo time evolution of the vertex number  $N_0$  and its associated probability distribution for a  $V = 32,000$  simplex simulation close to the critical line at  $\beta = 0.25$ . The tunneling behavior in the Monte Carlo time series, together with the double-peak structure in the probability distribution for the number of vertices  $P(N_0)$  constitutes strong evidence that the transition is first order in this region. The existence of the first-order transition precludes a continuum limit and indeed the observation of a similar structure at  $\beta = 0$  was the original motivation for introducing a measure term.

As we increase  $\kappa$  we observe that the latent heat of the transition, as measured by the separation in the two peaks in the probability distribution  $P(N_0)$  decreases and the structure of the susceptibility plots changes. If one fixes  $\kappa$  one observes a broad peak centered at  $\beta_{c1}$  followed by a much narrower peak at  $\beta_{c2}$  with  $\beta_{c2} > \beta_{c1}$ , Fig. 3. For  $\beta > \beta_{c2}$ ,

TABLE I. Pseudotransition point  $\kappa_c(\beta_c)$  obtained from fixed  $\beta$  ( $\kappa$ ) scan of the susceptibilities  $[\chi(\log q)]$  at target volume  $V = 32$  k vs corresponding estimates of the critical point  $\hat{\kappa}_c(\hat{\beta}_c)$  determined from the average radius  $r_{\text{avg}}$ .

$\beta$	$\kappa_c$	$\hat{\kappa}_c$
1.00	-0.89(1)	-0.894(6)
0.50	0.75(1)	0.756(6)
0.25	1.61(2)	1.606(6)
$\kappa$	$\beta_c$	$\hat{\beta}_c$
2.0	0.14(1)	0.144(6)
2.5	0.00(1)	0.006(6)
3.0	-0.13(1)	-0.13(1)
3.5	-0.25(1)	-0.244(6)
4.0	-0.36(1)	-0.35(1)
4.5	-0.46(1)	-0.46(1)
5.0	-0.56(1)	-0.56(1)

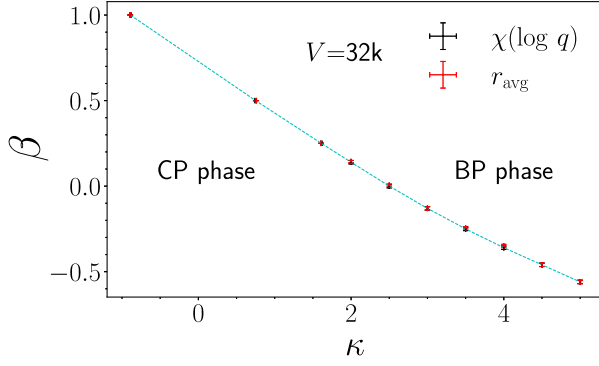


FIG. 5. Phase diagram of the pure gravity model with the combinatorial triangulation. Transition line separates the collapsed (CP) phase and the branched polymer (BP) phase.

the system is clearly in the branched polymer phase, while for  $\beta < \beta_{c1}$ , the system is clearly in the crumpled phase. The separation  $\Delta\beta$  between the two critical points narrows down as the volume is increased. In our lattice analysis, we have used  $\beta_{c2}$  as our best estimate for the pseudocritical point  $\beta_c$ .

To complement this determination of the critical point, we have also studied the mean radius of the discrete geometry which is defined by

$$r_{\text{avg}} = \frac{1}{N_4} \left\langle \sum_r r N_3(r) \right\rangle_T, \quad (6)$$

where  $N_3(r)$  is the number of four simplices at geodesic distance  $r$  measured on the dual lattice from some randomly chosen origin. In Fig. 4 we show a plot of the mean radius  $r_{\text{avg}}$  vs  $\beta$  for several values of  $\kappa$ . Like the susceptibility plots, the signature of the first-order phase transition is also evident from the plot of the average radius  $r_{\text{avg}}$  of the simplicial universe. To find the critical coupling, we computed a numerical derivative of the radius as a function of  $\beta$  and identified the critical point  $\hat{\beta}_c$  as the point where this derivative is maximal. A list of transition points derived from this observable is added in the second column of Table I and shown to agree very well with the  $\beta_c$  values determined from the susceptibility of the measure term  $\chi_{\log q}$ . Notice that for the small- $\kappa$  regime, we have fixed the value of  $\beta$  and scanned in  $\kappa$  to search for a transition point. Whereas for the large- $\kappa$  regime, we have fixed  $\kappa$  and done a scan in  $\beta$  values.<sup>2</sup> Results obtained from different simulations are combined to produce the phase diagram in Fig. 5. The transition line separates the collapsed phase and the branched polymer phase. Properties of these two phases

<sup>2</sup>This was motivated by the schematic phase diagram known from the earlier studies [7], where the transition line shows a trend to asymptote to a negative  $\beta_c$  value at large  $\kappa$ . However, there is no guarantee that we will find a similar trajectory of the transition line in our analysis with the new measure term.

are further discussed in the subsequent sections, and results obtained seem to be consistent with the degenerate triangulation studies [7].

#### IV. HAUSDORFF DIMENSION

To compute the Hausdorff dimension  $D_H$  we assume that  $N_3(r)$  takes the scaling form

$$N_3(r) = N_4^{1/D_H-1} f(r/N_4^{1/D_H}). \quad (7)$$

Fitting to this form shows that the Hausdorff dimension in the branched polymer phase is consistent with the value of  $D_H = 2$  (Fig. 6) while in the collapsed phase, the extracted value of  $D_H$  from such fits is large, which is consistent with the continuum expectation of infinite Hausdorff dimension [18,19]. At small distances,  $N_3$  should grow as  $\sim r^{D_H-1}$  [18]. In practice, we have used this fact rather than data collapse on the scaling form to extract  $D_H$  close to the critical line on our largest lattice by fitting

$$N_3 = A r^{D_H-1} + B. \quad (8)$$

Figure 7 shows such a fit. For a single pair of  $(\kappa, \beta)$ , several such fits were performed and systematic errors were computed due to the choice of different fit ranges. Details of the error analysis for the computation of the Hausdorff dimension is similar to the error analysis of the spectral dimension computation which are discussed in the following section. The results presented are an ensemble average computed from 2000 thermalized configurations. The fit is performed at several fixed  $\beta$  and fixed  $\kappa$  to observe the variation in the Hausdorff dimension as we move from the collapsed phase to the branched polymer phase. The value of the Hausdorff dimension is strongly influenced by the distance from the critical line as can be seen in Fig. 8, which shows  $D_H(\beta)$  at a fixed  $\kappa = 4.0$ . From the rise of the value of  $D_H$  towards the left, it is evident that

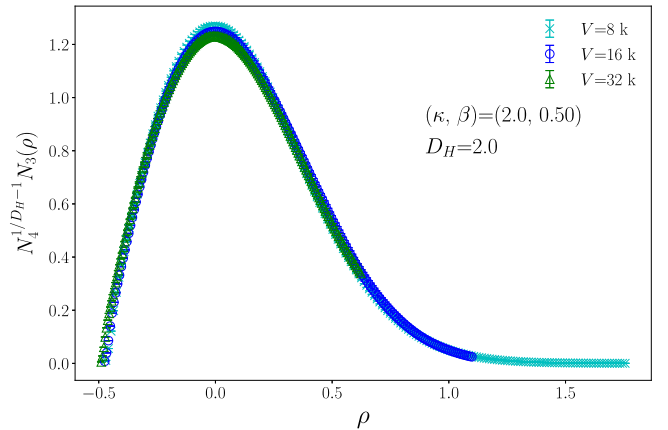


FIG. 6. Data collapse of the three-volume  $N_3(\rho)$  with scaled distance is consistent with  $D_H = 2.0$  in the BP phase.

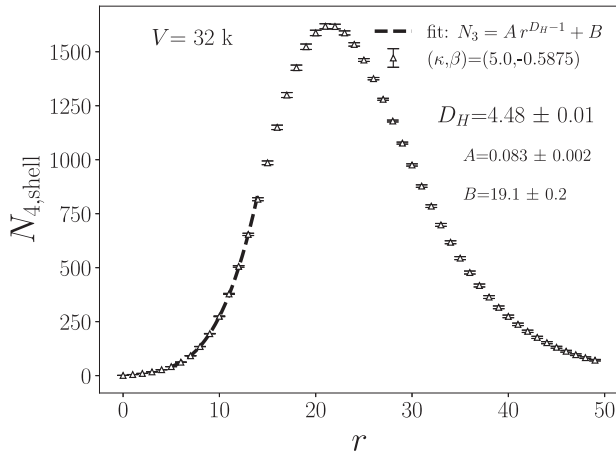


FIG. 7. Fit of the three-volume data at small distance.

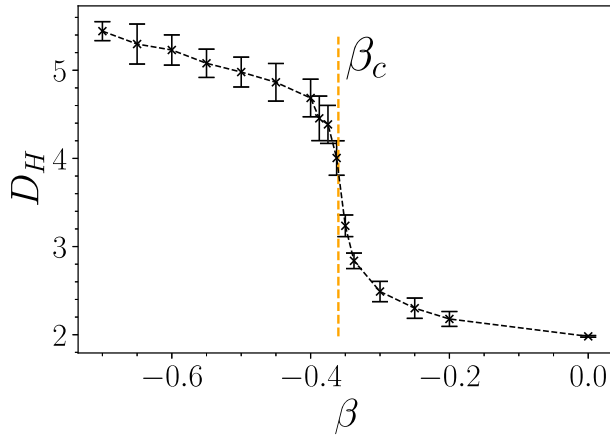
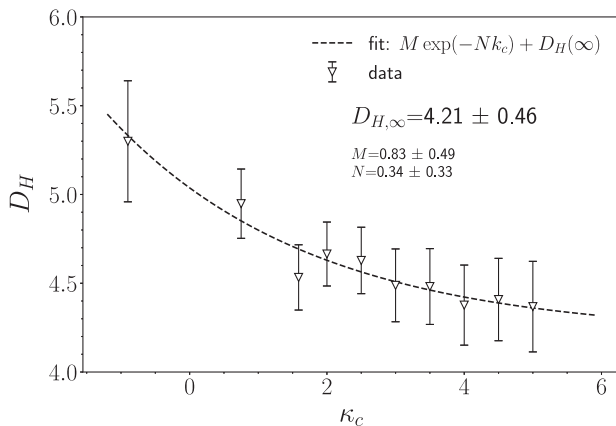
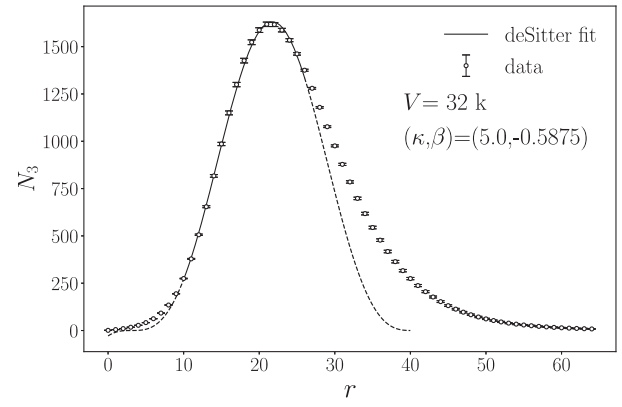

 FIG. 8. Variation in Hausdorff dimension  $D_H$  with  $\beta$  at  $\kappa = 4.0$  at  $V = 32$  K. Position of the critical coupling  $\beta_c$  derived from susceptibility is noted with the vertical line.

 FIG. 9. Fit to the extracted Hausdorff dimension  $D_H$  as a function of critical coupling along the transition line.


FIG. 10. Fit to the de Sitter solution of the three-volume distribution data.

as we probe deep into the collapsed phase, we get larger Hausdorff dimensions. Also clearly visible is that deep in the branched polymer phase on the right of the diagram, the value of  $D_H$  approaches the known value of 2.

In Fig. 9, we demonstrate the measured Hausdorff dimension along the critical line which also includes a fit of the form

$$D_H = M \exp(-N \kappa) + D_{H,\infty}. \quad (9)$$

Here,  $M$  and  $B$  are fit parameters and  $D_H \rightarrow D_{H,\infty}$  as  $\kappa \rightarrow \infty$ . We find  $D_{H,\infty} = 4.21 \pm 0.46$  which is consistent with the emergence of four-dimensional de Sitter space in this limit.

Encouraged by this, we have compared our three-volume distribution near the critical point at large  $\kappa$  with the (Euclidean) de Sitter solution.<sup>3</sup> The associated three-volume profile for the Wick rotated case takes the form of Eq. (10) [7,20,21]. An attempt to fit the three-volume data to the de Sitter solution is made in large  $\kappa_c$  Fig. 10, and the fit indicates that the average geometry at small to intermediate distances is consistent with de Sitter solution,

$$N_3(r) = \frac{3}{4} N_4^{3/4} \Gamma \cos^3 \left( \frac{r-b}{s_0 N_4^{1/4}} \right). \quad (10)$$

Here,  $s_0$ ,  $\Gamma$  and  $b$  are fit parameters. One can think of  $s_0$  as determining a relative lattice spacing for different values of the  $(\kappa, \beta)$ . We find a good matching of our data to the de Sitter solution starting from a small distance  $r$  up to about five steps beyond the maxima. The long tail of the distribution is likely a finite size effect [7].

<sup>3</sup>Solution of the Einstein's equation for a homogenous and isotropic universe described by the Friedmann-Lemaître-Robertson-Walker metric.

## V. SPECTRAL DIMENSION

Another measure of the fractal dimension for a fluctuating geometry is called the ‘‘spectral dimension’’  $D_S$ . It can be computed for a simplicial manifold  $\mathcal{M}$  using a random walk process. First, a simplex is randomly chosen in the triangulation. Then starting from that simplex, the random walk corresponds to successively moving from one simplex to one of its neighbors via a randomly selected face. This process is then iterated a large number of times for the same triangulation. To compute the spectral dimension, one records the number of times the walk returns to the starting simplex as a function of the diffusion time (number of steps of the random walk). By running several of these walks and averaging over starting points and over the ensemble of configurations obtained at some fixed  $\beta$  and  $\kappa$  we can obtain the probability of returning to the starting simplex  $P_r(\sigma)$  after  $\sigma$  steps. The spectral dimension is then defined from the relation,

$$D_S(\sigma) = -2 \frac{d \log \langle P_r(\sigma) \rangle}{d \log \sigma}. \quad (11)$$

The return probability is also a useful quantity that can be used to find the relative lattice spacing at different points on the transition line [7]. This is discussed in more detail in the Appendix.

In the branched polymer phase, we observe  $D_S = 4/3$ , which is consistent with theoretical expectations [22] while in the crumpled phase, it is large. At the critical point, we find  $D_S$  is not well-fitted by a constant but instead runs with scale  $\sigma$ . In Fig. 11, we show a plot of this running spectral dimension for  $V = 32$  K and  $\beta = -0.1375$ ,  $\kappa = 3.0$ .

We used 2000 thermalized configurations for the computation of the spectral dimension. Each random walk is performed up to 15,000 steps, and we choose 32,000 randomly chosen sources (starting point of the walk) per configuration. The fit is attempted over different ranges. Due to the finite volume of the lattices, the spectral dimension will increase and reach a maximum before

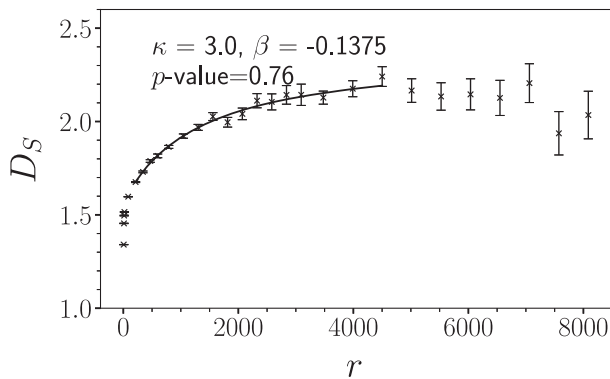


FIG. 11. Sample fit of the spectral dimension near the transition line in the phase space.

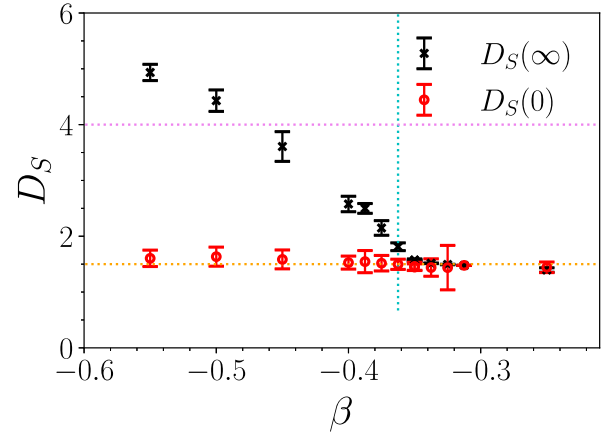


FIG. 12. UV [ $D_S(0)$ ] and IR [ $D_S(\infty)$ ] spectral dimension across transition at a fixed  $\kappa = 4.0$ . The vertical line denotes the position of the transition point, and the two horizontal lines denote the  $D_S$  value of 1.5 and 4 for comparison with the data.

decreasing. However, the number of steps needed to reach this maximum depends on the effective dimension of the manifold. We use data points up to the maximum value of the spectral dimension whenever possible. This amounts to choosing different fit ranges at different regions of the parameter space. The choice of the fit range is justified by tracking the  $p$ -value of the fits.

As in previous works [7,23], we found the following fit function best represents the data

$$D_S(\sigma) = a + \frac{b}{c + \sigma}. \quad (12)$$

The fit function yields estimates for the spectral dimension at small distances  $D_S(0)$  and also at large distances  $D_S(\infty)$ . A single-elimination jackknife procedure is used to compute the error bars, and the fit is performed for different fit ranges. Systematic errors due to the choice of the fit range

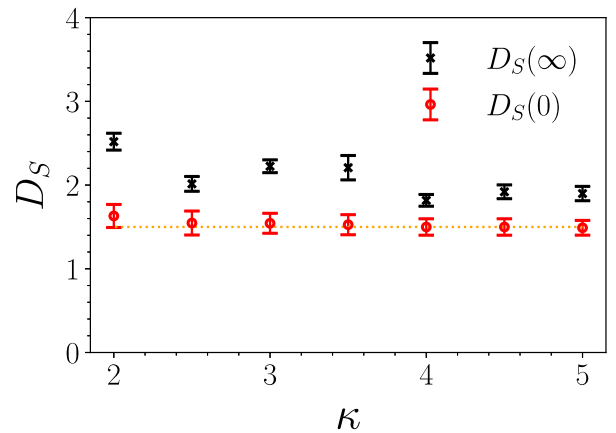


FIG. 13. UV [ $D_S(0)$ ] and IR [ $D_S(\infty)$ ] spectral dimension along the transition line. The horizontal line denotes the  $D_S$  value of 1.5 for the comparison.

are added in quadrature with the statistical error of the best fit used to compute the overall error. We use the metric ‘ $p$ -value’ to select reasonable fit ranges for the data. Figure 12 shows the variation of  $D_S(0)$  and  $D_S(\infty)$  across the transition line from the crumpled to the branched polymer phase, while Fig. 13 shows the variation of these quantities along the transition line. Analysis of the spectral dimension reveals that  $D_S$  runs to small ( $D_S \sim 1.5$ ) values in the UV, which is consistent with the earlier EDT studies [24], and CDT studies [25]. In the IR regime, the spectral dimension  $D_S(\infty)$  is larger with  $D_S(\infty)$  varying from 1.82–2.52. This scale dependence of the spectral dimension was also seen earlier in CDT [23], renormalization group approach [26], loop-quantum gravity [27] and in string theory models [28]. It needs to be clarified from our study whether the UV spectral dimension  $D_S(\infty)$  attains larger values for larger  $N_4$ . Larger volume simulations with combinatorial triangulations must be conducted to resolve the tension in the observed UV spectral dimension from our study with the results obtained from the degenerate combinatorial calculations [6].<sup>4</sup>

## VI. CONCLUSIONS

We have explored the phase diagram of the combinatorial Euclidean dynamical triangulation model of four-dimensional quantum gravity. The model contains two parameters—a bare gravitational coupling  $\kappa$  and a measure-parameter  $\beta$ . We find evidence for a critical line  $\kappa_c(\beta)$  that separates a crumpled phase from a branched polymer phase, which agrees with the results obtained from earlier studies [7,10]. While this line is associated with first-order phase transition for small  $\kappa$ , the transition softens with increased value of the coupling. An intermediate “crinkled” phase opens up in this regime, but we have focused our attention on the boundary between this region and the branched polymer phase in our analysis since this is the only place where we have observed consistent scaling that survives the large volume limit. When we refer to the critical point in our results, we always mean the boundary between the crinkled and branched polymer phases.

The focus of much of our work has been to compute the Hausdorff and spectral dimensions as we approach this

critical line from the crumpled phase. We find evidence that the Hausdorff dimension  $D_H$  along the critical line approaches  $D_H = 4$  as  $\kappa$  increases where it is possible to obtain increasingly good fits to classical de Sitter space. The spectral dimension  $D_S(s)$  is observed to run with scale  $s$  attaining values consistent with  $D_S(0) = \frac{3}{2}$  at short distances for all values of  $\kappa$ . These results are consistent with earlier work using degenerate triangulations and causal dynamical triangulation models and models using different measure terms [7,10,25]. However, our measurement of the spectral dimension at long distances  $D_S(\infty)$  barely exceeds  $D_S(\infty) \sim 2$ . This result is somewhat in tension with the earlier work. However, we show that  $D_S(\infty)$  depends strongly on the distance in parameter space from the critical line, which renders such measurements delicate and may explain this discrepancy. Large finite volume effects, also observed in earlier studies, make this measurement quite delicate.

## ACKNOWLEDGMENTS

We acknowledge Syracuse University HTC Campus Grid and NSF Grant No. ACI-1341006 for the use of the computing resources. S.C. was supported by DOE Grant No. DE-SC0009998.

## APPENDIX: RELATIVE LATTICE SPACING

In this work, we did not attempt to measure the renormalized gravitational constant, which determines the absolute lattice spacing. Instead, we have used the relative lattice spacing obtained from the return probability. Two different methods of finding the gravitational constant in the context of the Euclidean dynamical triangulation can be found in the two recent papers by Laiho *et al.* [8,9]. In Fig. 14(a), we show the return probability at several different points along the critical curve for  $V = 32$  K, and in Fig. 14(b), it is shown that the curves at different points in the critical line of the phase diagram can be collapsed onto a single curve by rescaling the step size (diffusion time of the random walk)  $\sigma$ . Rescaling of the step  $\sigma = \sigma_r a_r^2$  can be interpreted as yielding a relative lattice spacing  $a_r$  as  $\kappa$  varies along the critical curve. Values of the relative lattice constant  $a_r$  are noted in Table II and are consistent with the previous work by Laiho *et al.* Namely, they reveal that as  $\kappa$  approaches infinity, the corresponding lattices get finer [7]. Hence, for a fixed target volume  $V$ , the physical volume is smaller at larger  $\kappa_c$ , and it is likely that the results obtained would suffer a greater finite size effect in that region.

<sup>4</sup>In this study, we did not take the double scaling limit of the spectral dimension as suggested by Laiho *et al.* [7] by simultaneously taking lattice spacing to zero and lattice volume to infinity. Performing such an extrapolation might be important for extracting a continuum value for the UV spectral dimension.

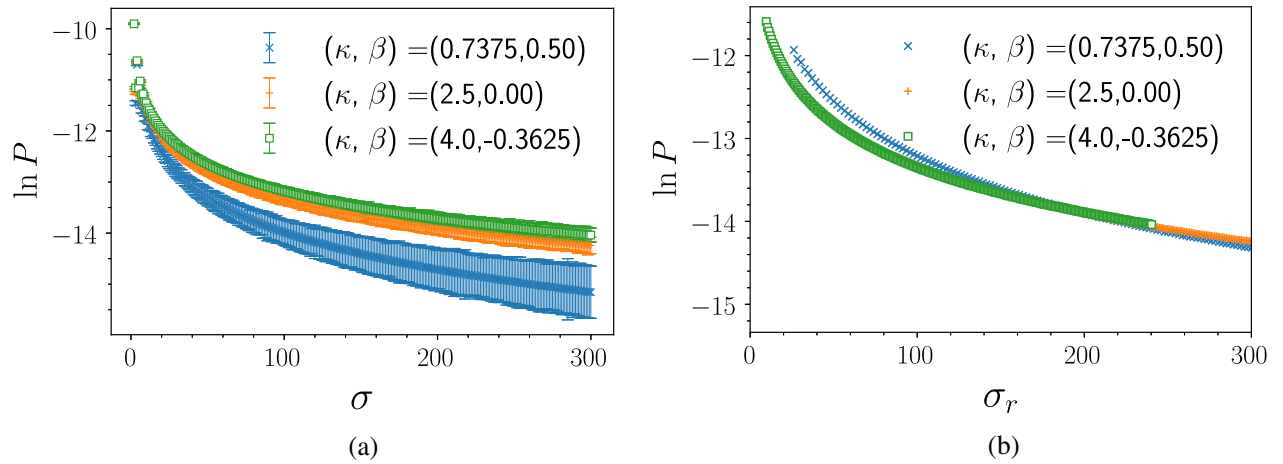


FIG. 14. Return probability at different points in the critical line at lattice volume  $V = 32$  k (a) with respect to diffusion step ( $\sigma$ ), (b) with respect to rescaled diffusion step ( $\sigma_r$ ). The scaling allows to find relative lattice spacing along the transition line. Associated error bars are not shown in the right-hand figure to demonstrate the superimposed data from different points in the transition line.

TABLE II. Relative lattice spacing  $a_r$ , as the  $\kappa$  is varied along the transition line.

$\kappa$	-0.90	-0.7375	1.5625	2.0	2.5	3.0	3.5	4.0	4.5	5.0
$a_r$	1.5	1.475	1.135	1.05	1	0.935	0.92	0.895	0.87	0.86

- [1] A. Ashtekar and E. Bianchi, *Rep. Prog. Phys.* **84**, 042001 (2021).
- [2] R. Loll, *Classical Quantum Gravity* **37**, 013002 (2020).
- [3] S. Weinberg, *General Relativity* (University Press, Cambridge, 1979).
- [4] M. Niedermaier and M. Reuter, *Living Rev. Relativity* **9**, 5 (2006).
- [5] J. Ambjørn, A. Görlich, J. Jurkiewicz, and R. Loll, *Int. J. Mod. Phys. D* **22**, 1330019 (2013).
- [6] J. Laiho and D. Coumbe, *Phys. Rev. Lett.* **107**, 161301 (2011).
- [7] J. Laiho, S. Bassler, D. Coumbe, D. Du, and J. T. Neelakanta, *Phys. Rev. D* **96**, 064015 (2017).
- [8] M. Dai, J. Laiho, M. Schiffer, and J. Unmuth-Yockey, *Phys. Rev. D* **103**, 114511 (2021).
- [9] S. Bassler, J. Laiho, M. Schiffer, and J. Unmuth-Yockey, *Phys. Rev. D* **103**, 114504 (2021).
- [10] J. Ambjørn, L. Glaser, A. Görlich, and J. Jurkiewicz, *J. High Energy Phys.* **10** (2013) 100.
- [11] S. Catterall, J. Kogut, R. Renken, and G. Thorleifsson, *Phys. Lett. B* **366**, 72 (1996).
- [12] J. Ambjørn and J. Jurkiewicz, *Phys. Lett. B* **335**, 355 (1994).
- [13] T. Regge, *Il Nuovo Cimento* (1955–1965) **19**, 558 (1961).
- [14] K. S. Thorne, C. W. Misner, and J. A. Wheeler, *Gravitation* (Freeman, San Francisco, 2000).
- [15] D. Boulatov, V. Kazakov, I. Kostov, and A. A. Migdal, *Nucl. Phys.* **B275**, 641 (1986).
- [16] V. A. Kazakov, *Phys. Lett.* **119A**, 140 (1986).
- [17] S. Catterall, *Comput. Phys. Commun.* **87**, 409 (1995).
- [18] J. Ambjørn and J. Jurkiewicz, *Nucl. Phys.* **B451**, 643 (1995).
- [19] D. Coumbe and J. Laiho, *J. High Energy Phys.* **03** (2015) 151.
- [20] J. Ambjørn, A. Görlich, J. Jurkiewicz, and R. Loll, *Phys. Rev. D* **78**, 063544 (2008).
- [21] L. Glaser and R. Loll, *C.R. Phys.* **18**, 265 (2017).
- [22] T. Jonsson and J. F. Wheeler, *Nucl. Phys.* **B515**, 549 (1998).
- [23] J. Ambjørn, J. Jurkiewicz, and R. Loll, *Phys. Rev. Lett.* **95**, 171301 (2005).
- [24] J. Laiho, S. Bassler, D. Coumbe, D. Du, and J. Neelakanta, *Acta Phys. Pol. B Proc. Suppl.* **10**, 317 (2017).
- [25] D. N. Coumbe and J. Jurkiewicz, *J. High Energy Phys.* **03** (2015) 151.
- [26] O. Lauscher and M. Reuter, *J. High Energy Phys.* **10** (2005) 050.
- [27] L. Modesto, *Classical Quantum Gravity* **26**, 242002 (2009).
- [28] P. Hořava, *Phys. Rev. Lett.* **102**, 161301 (2009).